Diamond & Related Materials 19 (2010) 972–975

Contents lists available at ScienceDirect

Diamond & Related Materials

journal homepage: www.elsevier.com/locate/diamond

Local boron doping quantification in homoepitaxial diamond structures

D. Araújo [a,*], P. Achatz [b], R. El Bouayadi [c], A.J. García [a], M.P. Alegre [a], M.P. Villar [a], F. Jomard [d], E. Bustarret [a,b]

[a] Dpto Ciencia de los Materiales, Facultad de Ciencias, Universidad de Cádiz, 11510 Puerto Real (Cádiz), Spain
[b] Institut Néel, CNRS-Université Joseph Fourier, 25 av. des Martyrs, 38042-Grenoble, France
[c] Faculté Pluridisciplinaire de Nador, B.P. 300 Selouane 62700, Morocco
[d] CNRS-gemac, Université de Versailles St. Quentin, 92195 Meudon Cedex, France

ARTICLE INFO

Available online 1 March 2010

Keywords:
Diamond
Boron doping
Homoepitaxy
TEM
HAADF

ABSTRACT

The capability of transmission electron microscopy (TEM) using the high angle annular dark field mode (HAADF, also labelled *Z*-contrast) to quantify boron concentration, in the high doping range between $10^{19}\,cm^{-3}$ and $10^{21}\,cm^{-3}$, is demonstrated. Thanks to the large relative variation of atomic number *Z* between carbon and boron, doping concentration maps and profiles are obtained with a nanometer-scale resolution. A novel numerical simulation procedure allows the boron concentration quantification and demonstrates the high sensitivity and spatial resolution of the technique.

1. Introduction

Up to date homoepitaxial diamond demonstrated capabilities to yield high power, short wavelength or high frequency devices, as well as superconducting or single photon-emitting materials. This requires a rigorous structural and chemical control of the microwave plasma-assisted chemical vapor deposition (MPCVD) of diamond. Although the development of advanced electronic devices such as delta-doped field effect transistors [1] will require optimizing the structure of each epilayer, doping profiles and/or defects distribution were rarely evaluated down to the nano- and microstructural level. The use of the *Z*-contrast mode of the scanning transmission electron microscope (STEM), also named HAADF (high angle annular dark field), is well known to allow atomic resolution [2]. Thus, individual atoms at interfaces as isolated boron atoms in carbon nanostructures [3] or concentration profiles in nanostructures have been demonstrated. So far, the method has yielded either concentrations in the alloying range or individual atoms identification at atomic resolution, but seemed insufficiently sensitive for doping level determination in Si or III–V compounds. The low *Z*-number of carbon allows to increase the relative *Z* variation when dopant entities are introduced. A new method to assess at the nanometric scale the doping level in boron-doped diamond epilayers is proposed in the present contribution. We shall first describe the method, and then apply it to a particular stack of diamond epilayers also characterized by SIMS.

Among the transmission electron microscopy (TEM) modes, several allow to assess chemical analysis of pseudomorphic epilayers. The high resolution mode allows to observe atomic columns and atomic strain variations which lead to composition variations through the stress–strain relationship [4,5]. More frequently used for local chemical analysis in combination with TEM, the X-ray detection (EDX) and electron energy loss modes (EELS or even Gatan Image Filtering for individual element maps) allow to identify the presence of chemical elements [6]. However, their sensitivity is low and micrographs with a resolution below 10 nm are very difficult to obtain. On the other hand, high angle annular dark field (HAADF) is, in STEM (scanning transmission electron microscopy) mode, highly sensitive to the atomic number. HAADF images provide unique and powerful capabilities for characterization of structural morphology in semiconductor device structures. Simulation should be used to quantify the concentration of chemical elements and different models with atomic resolution, i.e. with an electron beam spot size around 0.1 nm, were published recently [7]. Current STEM image calculations may be classified into two groups: (i) the Bloch wave method [8,9] and (ii) the multi-slice method. Methods related to the second group were more extensively used for high resolution quantitative analysis [10]. They are based on the Fast Fourier Transform (FFT) multi-slice algorithms [11,12], where a wave function within the sample and its Fourier Transform are evaluated simultaneously. The high angle integration of the wave function gives the TDS (thermal diffused scattering) signal of the HAADF mode.

However, such high "atomic" resolution conditions are very difficult to reach experimentally in standard TEM equipments. It requires a specific installation of the TEM to avoid all kinds of mechanical and electromagnetic perturbations. The use of nanometric, but not atomic, resolution range is much less demanding. Modelization codes for high resolution are not valid anymore and a specific code should be developed. For this purpose, a basic methodology with theoretical/numerical simulations has been carried out. A simple multi-slice method, based on simulations of the HAADF intensity scattered by a heterogeneous sample is presented below.

* Corresponding author. Tel.: +34 956 01 6427; fax: +34 956 01 6288.
E-mail address: daniel.araujo@uca.es (D. Araújo).

0925-9635/$ – see front matter.
doi:10.1016/j.diamond.2010.02.043

Such calculations can, in addition, advantageously be undertaken following a tomographical approach, avoiding the huge number of projections required for a reasonable 3D investigation.

2. HAADF simulation methodology

HAADF experiments were performed under scanning transmission electron microscopy (STEM) mode of a TEM by focusing the electron beam probe on a point of the specimen and scanning it afterwards. The signal was collected on an annular detector, with a collecting angle typically from 60 mrad to 200 mrad, located at the focal plane of the objective length. The collecting angle can be optimized by changing the camera length in order to avoid Bragg diffraction spots to illuminate the detector. The signal collected at high angles results from incoherent scattering with thermally excited atoms of the analyzed sample. Indeed, the interaction of a high energetic electron with a phonon modifies slightly the electron energy – i.e. its **k** wave vector norm – applying the energy conservation principle but, the momentum conservation implies a high angular variation of the **k** vector. This means that such scattered electrons change strongly their direction and therefore can be collected at high angles with the annular HAADF detector. Thus, these electrons do not contribute to the Bragg diffraction (BS), i.e. elastic electrons intensity is reduced by the effect of the temperature as electron is diffused at higher angles [7]. This is usually expressed by the Debye–Waller factor that reduces the electron intensity [13]. The "lost" electrons are labelled "thermally diffuse scattering (TDS)". This phonon-related scattering is dominant at angles above values around 20 mrad depending on the material atomic number. As shown in Fig. 1a, at those collecting angles, the total collected intensity is dominated by TDS and can be described by the convolution of the probe intensity function (nearly a Gaussian depending on the column parameters) and the scattering object function [14,15].

While the TDS intensity must be integrated over the detector collecting angle for each atom crossed by the electron beam to obtain the HAADF signal, the BS intensity participates in the diffraction spot intensities. In the following, low resolution (<1 nm) multi-slice calculations of the HAADF intensities are presented for boron-doped/undoped diamond epilayers.

First, we calculate the I^{TDS} and I^{BS} intensities of all elements likely to be present in the sample. This will enable us, thereafter, to generate a series of contrasted images in order to compare them with the experimental image. The I^{TDS} and I^{BS} intensities are calculated in the interval of spatial frequencies (s) corresponding to the two angles of detection of the annular detector $2\theta_{min}$ and $2\theta_{max}$. The detection angles are chosen in the manner that I^{BS} is negligible in comparison to I^{TDS}.

Using several experimental HAADF images, a simplified geometrical 3D shape of the analyzed zone is proposed for simulation. The chosen volume is afterwards discretized in a small elementary volumes (a cubic whose edge length is generally equal to one pixel) as shown in Fig. 1a. Knowing the exact size of each layer of the stack and their positions in the matrix, each elementary volume is associated with determined chemical composition. SIMS investigations provide a first input of the chemical composition and on the other hand the TDS and BS intensities scattered by each element present are calculated versus s.

When the centre of the electron beam is located at one defined position (pixel (i,j)), it illuminates the surface of several elementary volumes of the specimen which are inside the probe (Fig. 1a) depending on the spot size and elastic scattering spreading of the incident e-beam. Then, the sum of all the elementary volumes bombarded by the electronic probe is considered for the calculation of the intensity diffused attributed to the pixel (i,j). Indeed, the intensity of the probe is distributed in a Gaussian way on all the elements. The total intensity (I^{TDS} and I^{BS}) diffused by each elementary volume is thus modulated by the Gaussian function of the probe. The total intensity diffused by elementary volume corresponding to the pixel (i,j) (centre of the probe) is simply obtained by calculating the average of all the pixels illuminated by the probe. Each pixel is sending a number of electrons depending on the composition which is introduced as an input (and the corresponding

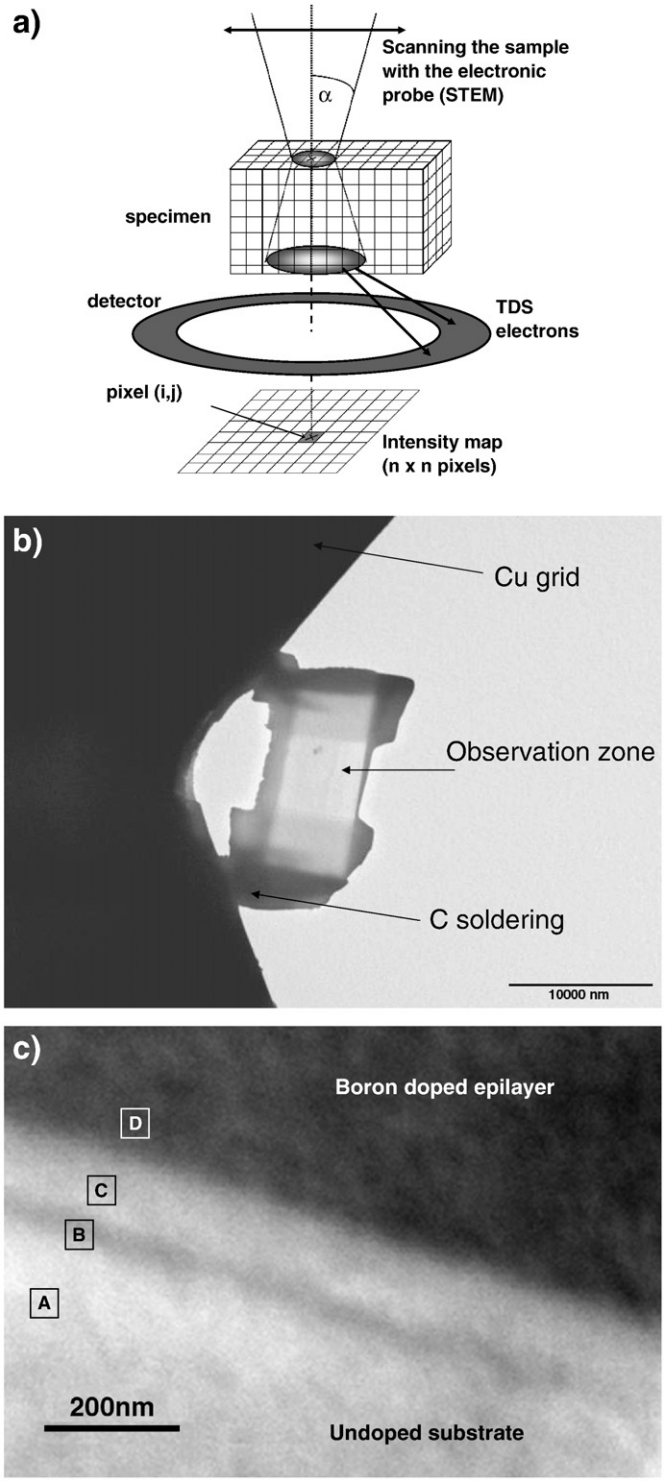

Fig. 1. (a) Schematic description of the HAADF image formation when the e-beam is located at one position. As the beam scans the sample surface, calculations are carried our point by point; (b) general view of a FIB-prepared diamond specimen, ready for STEM-HAADF observations; (c) STEM-HAADF micrograph near the substrate–layer interface. The doped layers appear darker with respect to the undoped substrate. The layers are labelled by the letters in squares: "A" the undoped substrate, "B" boron enriched part of the buffer, "C" poorer boron part of the buffer, "D" the highly doped CVD grown layer.

$I(s)$ curve is calculated), and then this is integrated over the detector collection angle (see Fig. 1a). For each probe position (pixel (i,j)), this operation is repeated at each depth z of the sample (multi-slice method). In this calculation, the beam spreading with the depth (noted b) is also considered by using the Goldstein equation [16]. Then, the total intensity scattered layer by layer (column (i,j)) is calculated and then summed. This value is attributed to the beam position corresponding pixel (see gray pixel in Fig. 1). Then the HAADF image is formed by scanning the sample surface with the probe position. It should be noted that the electron beam size spread crossing the sample. The probe's diameter becomes broader and the number of illuminated pixels becomes larger, increasing the computing time considerably. Finally, a feed-back on the composition is performed to ensure the convergence between the experimental and calculated profiles.

3. Experimental results and discussion

3.1. Experimental

The sample has been grown by MPCVD in a vertical silica tube reactor as described elsewhere [17] on a (100)-oriented HPHT type Ib diamond substrate. After a 2 hour-long pure hydrogen plasma at 880 °C, a thin non intentionally doped "buffer" layer was grown at 830 °C first from 0.25% CH_4 in purified H_2, and then the methane concentration was raised to 4% and B_2H_6 (B/C = 1800 ppm) was added to the gas mixture without turning off the plasma, and a thicker (almost 4 μm) heavily boron-doped layer was grown.

Because diamond is the hardest known material, specimen preparation for cross-section TEM observation was made using a Focused Ion Beam in a Dual Beam Scanning electron microscope (FIB-Dual Beam). Fig. 1b shows the final sample preparation after being solded using carbon gas source on a Cu grid. The surface of the preparation was oriented toward [110] direction, parallel to the substrate edge. HAADF experiments are performed under scanning transmission electron microscopy (STEM) mode of a TEM (JEOL 2010F) by focusing the electron beam probe on a point of the specimen and scanning it afterwards. The signal is collected on an annular detector, with a collecting angle typically from 60 mrad to 200 mrad (8 mm camera length), located at the focal plane of the objective length. The collecting angle can be optimized by changing the camera length in order to avoid Bragg diffraction spots to illuminate the detector.

The SIMS profile was collected in a Cameca IMS 4f apparatus and ^{11}B, ^{12}C, ^{14}N, $^{11}B^{12}C$, $^{12}C^{14}N$ and ^{28}Si masses were detected using 10 keV Cs^+ ions and a 4.5 keV extraction potential. A diamond reference implanted with 2×10^{15} B/cm^3 was measured in the same run to calibrate (within 20% uncertainty) the boron atomic density deduced from the $^{11}B^{12}C$ signal, while the nitrogen concentration in the substrate was estimated (within 50%) from previous calibrations. The depth scale was deduced from the final sputtered crater depth.

3.2. SIMS profile and HAADF results

As shown in Fig. 2a, the film contained about 1.3×10^{21} B/cm^3 and was about 3.7 μm-thick. Because of residual boron left over on the silica walls of the reactor from previous heavily doped runs, the nominally undoped "buffer" layer was found to be boron doped at 10^{18} B/cm^3 level, especially in the first 50 nm near the interface where a concentration peak reaches $3.5\cdot10^{18}$ cm^{-3}. This interface of the roughly 100 nm-thick buffer layer with the substrate is clearly visible in the SIMS profile for nitrogen, where the concentration is a factor of five lower in the CVD film than in the HPHT substrate. It can also be seen that upon introduction of diborane, the boron concentration has risen steeply by 3 orders of magnitude, with a minimum width of 15 nm/decade.

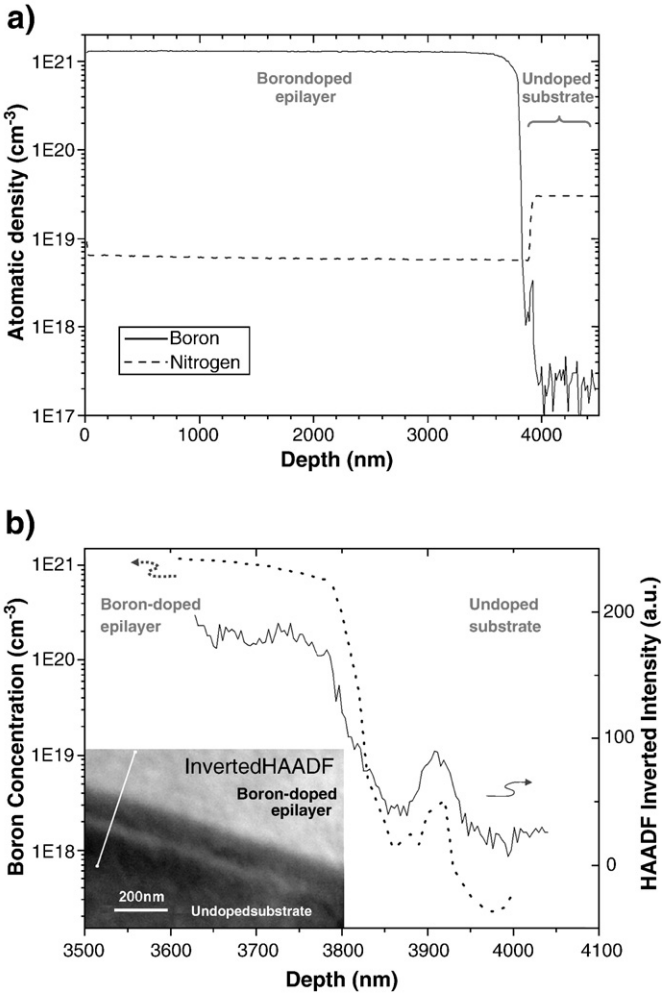

Fig. 2. (a) SIMS profile of boron and nitrogen species of the homoepitaxial structure, (b) detail near the epilayer–substrate interface of the SIMS and inverted HAADF profiles. Dashed line (SIMS) corresponds to the left hand scale while the continuous one to the right hand scale (HAADF). In the inset the respective inverted HAADF micrograph with the location of the intensity profile is shown. The depth axis corresponds to the distance along the white line on the cross-section micrograph of the inset.

Fig. 1c shows the HAADF micrograph. The lower Z-number zone, i.e. the doped epilayer, diffuses fewer electrons according to the atomic scattering factor behaviour [18,19]. The undoped region, with a higher average Z-number, corresponds then to the white region and the boron-doped regions are darker. Thus, the HAADF profile is inverted with respect to the SIMS one. For the sake of comparison, an inverted contrast micrograph is shown with its respective intensity profile in Fig. 2b. The dashed curve corresponds to the SIMS profile and the continuous line to the inverted HAADF profile. The observed correspondence demonstrates that HAADF can qualitatively detect the presence of boron in the 10^{20} cm^{-3} range. Squares with letters label regions in Fig. 1c. "A" corresponds to the undoped substrate, "B" to the beginning of the CVD growth. Plasma-induced chemical transport from the boron-rich walls induced an undesired incorporation of boron in the beginning of the process. Therefore, "B" + "C" layers correspond to the buffer layer, the "C" layer being only slightly boron doped. "D" corresponds then to the highly boron-doped epilayer (see Fig. 2b).

The advantage of this technique is the possibility to improve significantly the spatial resolution. Depth and lateral variation of the boron composition can be revealed below the nm-scale. The present micrograph shows a slight lateral boron concentration modulation. However, on the studied sample, some curvature of the substrate

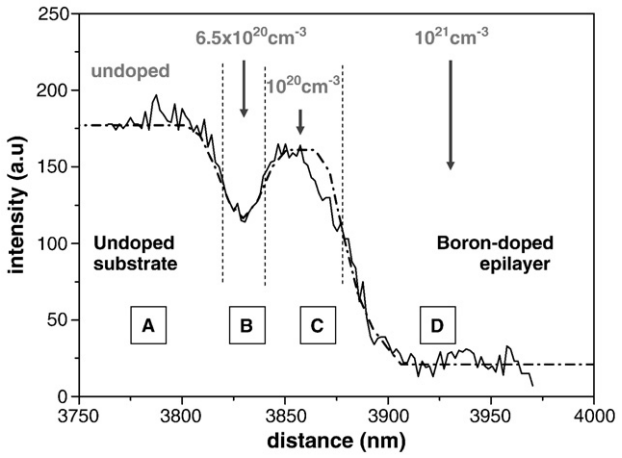

Fig. 3. Experimental and simulated HAADF profiles. Note that a direct contrast is used. Then boron-doped layer shows a lower intensity. The layer labelled with a letter is shown in reference to Fig.1c.

surface was observed with a respective μm-range variation of the interfacial boron related peak. In some other sample regions, the layer "B" related to the peak intensity change or boron is shown to be present in the whole buffer (layer "B + C"). However, to quantify the HAADF profile, more detailed simulations are required.

3.3. HAADF simulation results

Fig. 3 shows the experimental and simulated (in dashed line) HAADF intensity profiles in direct contrast, i.e. the doped layer is darker or with a lower intensity. A spot size of 5 nm and a sample thickness of 200 nm were used for the calculation. The sample thickness was determined using the plasmon peak in electron energy loss spectroscopy (EELS). Indeed, this value is important to evaluate the high energy electron incident beam spread. Quantification of those two parameters varies the bent of the calculated profile between layers. The lower are the thickness and spot size, the sharper become the profile between layers. The corresponding layer notation used in Fig. 2 is also indicated. To fit the experimental profile the values using the methodology of calculations described above, boron doping of 6.5×10^{20} and $10^{20}\,cm^{-3}$ have been introduced in the simulations. A good correspondence can be then observed between both profiles. To improve the sensitivity of the technique, i.e. to assess lower doping levels, signal noise should be reduced. This is possible either by integrating the experimental profile on a "thicker" line i.e. averaging several profiles or using a lower scan rate. One order of magnitude can be probably reached.

However, the deduced boron doping values do not correspond to the SIMS boron concentrations. As mentioned above, the experimental profile is found to vary along the 10 μm sample preparation. Other FIB-Dual Beam preparations were also observed showing also this change. Probably due to the very high doping, the sample is somewhat bent. Variations of the boron incorporation were found to occur, as the HAADF profile varies, depending on the change of orientations of the substrate–layer interface resulting from this bending. Thus, to obtain a comparison between both techniques, HAADF should be measured at the same place of the SIMS. The latter being a destructive method, the HAADF must be carried out before SIMS. However, a clear enrichment in boron is shown by both techniques. The amount of this enrichment varies depending the location on the sample surface. More studies are in progress to understand such behaviour.

4. Conclusion

A new numerical simulation method of the HAADF intensity calculation is reported. The method is applied to doping in diamond epilayers. A high spatial resolution and a relatively high chemical sensitivity are shown. Due to the large relative Z variation in diamond epilayers when dopants are introduced, HAADF is a very powerful technique to investigate spatial boron distribution in diamond layers. In particular, this technique is shown to be highly useful to control the boron incorporation in device structures as for example in delta-doped transistors. Sensitivities around $10^{20}\,cm^{-3}$ with an nm-scale spatial resolution are demonstrated.

Acknowledgments

We thank the Ministerio de Ciencia e Innovación (MICINN) of the Spanish Government for funding under Grant No. TEC2009-11399. We are also grateful for the use of the Central Electron Microscopy Facilities of the University of Cádiz.

References

[1] E. Kohn, A. Denisenko, Thin Solid Films 515 (2007) 4333.
[2] J. Pizarro, P.L. Galindo, E. Guerrero, A. Yáñez, M.P. Guerrero, A. Rosenauer, D.L. Sales, S.I. Molina, Appl. Phys. Lett. 93 (2008) 153107.
[3] U. Bangert, M.H. Gass, A.L. Beloch, R.R. Nair, J. Eccles, SBDD XIV, March 2009 Hasselt, Belgium.
[4] M.J. Hytch, E. Snoeck, R. Kilaas, Ultramicroscopy 74 (1998) 131.
[5] E. Sarigiannidou, E. Monroy, B. Daudin, J.L. Rouvière, A.D. Andreev, Appl. Phys. Lett. 87 (2005) 203112.
[6] R.F. Klie, I. Arslan, N.D. Browning, J. Electron. Spectr. Rel. Phenom. 143 (2005) 105.
[7] M. Shiojiri, T. Yamazaki, JEOL News 38 (2003) 54;
M. Shiojiri, T. Yamazaki, J. Microsc. 223 (2006) 172.
[8] P.D. Nellist, S.J. Pennycook, Ultramicroscopy 78 (1999) 111.
[9] G.R. Anstis, D.Q. Cai, D.J.H. Cockayne, Ultramicroscopy 94 (2003) 309.
[10] E.J. Kirkland, R.F. Loane, J. Silcox, Ultramicroscopy 23 (1987) 77.
[11] K. Ishizuka, Ultramicroscopy 90 (2002) 71.
[12] Private communication of P. Galindo
[13] R.F. Klie, Y. Zhu, Micron 36 (2005) 219.
[14] P.D. Nellist, S.J. Pennycook, Advances in Imaging and Electron Physics, Chapter 2, Ed. Academic Press0-12-014755-6, 2000.
[15] E. Abe, JEOL News 38 (2003) 63 or see also A. Guinier, X-Ray Diffraction in Crystals, Imperfect Crystals and Amorphous Bodies (Dover, Mincola, NY, 1994).
[16] D.B. Williams, C.B. Carter, Transmission Electron Microscopy, Plenum Press, New York978-0-387-76500-6, 1996.
[17] T. Klein, P. Achatz, J. Kacmarcik, C. Macenat, F. Gustafsson, J. Marcus, E. Bustarret, J. Pernot, F. Omnès, B. Sernelius, C. Person, A. Ferreira da Silva, C. Cyterman, Phys. Rev. B 75 (2007) 165313.
[18] D. Araújo, R. El Bouayadi, M. Gutiérrez, C.E. Pastore, M. Hopkinson, Mat. Sci. Eng. B 165 (2009) 88.
[19] E.J. Kirkland, R.F. Loane, J. Silcox, Ultramicroscopy 23 (1987) 77.